IAC–21–C1.1.7

Bearing-Only Navigation for proximity operations on Cis-lunar Non-Keplerian orbits

Michele Ceresoli
Politecnico di Milano, Italy - michele.ceresoli@mail.polimi.it

Giovanni Zanotti
Politecnico di Milano, Italy - giovanni.zanotti@polimi.it

Michèle Lavagna
Politecnico di Milano, Italy - michelle.lavagna@polimi.it

In the next years many scientific and demonstration missions will target the cislunar environment to consolidate existing technologies and foster the development of new space systems to support a future human exploration of Mars. Among those, the Lunar Orbital Platform Gateway (LOP-G) will operate as a long-term modular infrastructure in deep-space, offering services to both manned and unmanned missions to the Moon. To safely accomplish many of its tasks, rendezvous and docking/undocking operations must be reliably performed on highly non-Keplerian orbits. However, despite rendezvous and relative navigation are well-known for Earth-centred missions, no autonomous proximity operation has ever been performed in the cislunar domain. Within this framework, the paper assesses the applicability of Bearing-Only measurements to perform relative navigation between distant heterogeneous non-Keplerian orbits. Starting from the absolute motion, a useful discrete-time approximation of the non-Keplerian relative dynamics is presented to support the development of a computationally efficient Guidance, Navigation and Control (GNC) architecture based on a Shrinking Horizon - Model Predictive Control (SH-MPC) strategy. The outcomes of two different test scenarios are critically discussed to prove the effectiveness of the proposed method and highlight potential solutions that enhance the filter observability with minimum fuel consumption.

Keywords: Relative Non-Keplerian Dynamics, Bearing-Only Navigation, Shrinking Horizon - Model Predictive Control

Abbreviations:

DRO	Distant Retrograde Orbit	MPC	Model Predictive Control
LEO	Low Earth Orbit	SH	Shrinking Horizon
GNC	Guidance, Navigation and Control	STM	State Transition Matrix

1. Introduction

The latest decades have seen a renewed interest in Moon exploration missions, due to the envisaged roadmaps that define the lunar system as a perfect training environment for the development and advancement of space system technologies to support the human Mars exploration. Indeed, in such direction joint efforts are being performed by many space agencies to realise infrastructures to support the upcoming technological demonstration mission that will explore the Moon, such as GNSS constellations or modular space stations. Concerning the latter challenge, the Lunar Orbital Platform Gateway (LOP-G) is for certain among the most ambitious and interesting project, that will enable the possibility to have astronauts medium-term permanence in the cis-lunar environment. Its construction will be performed following a modular assembly approach, starting from the first modules in the mid-20s, through a series of mission within the NASA program Artemis. Starting from its assembly and continuing during the operational years, the Gateway will require the capabilities to perform docking and undocking operations, for which rendez-vous with different transportation spacecraft will be performed, to provide cargo, supply, scientific experiments or astronauts themselves. Particularly basic Guidance Navigation and Control

functionalities are needed by the avionic system onboard the involved agents and the possibility to increase the autonomy level of such system is a huge opportunity to reduce costs and human intervention. A great deal of experience has been gained by the international space community in the more familiar *Low Earth Orbit* environment through the ISS program, but no experiment at all has been conducted in the cis-lunar Non-Keplerian one.

A very promising technique that is able to provide autonomous GNC capabilities to spacecraft employing limited sensing resources is found in the *Bearing-Only Navigation*, whose goal is the exploitation of the relative line-of-sight vector measurement only to reconstruct the complete relative state vector. The attractiveness of such technique resides in the very limited sensors requirement in terms of mass, power and costs, which makes it suitable practically to all spacecraft classes, from cargo modules down to nanosatellites, such as CubeSats. The associated downsides, which make it little appealing in some terms, are the limited reduced observability capabilities.

Such reduced observability performances have been studied in the last decade in depth for their application in *LEO* scenarios by Woffinden [1] and Grzymisch [2], proving that the execution of orbital manoeuvres capable of providing a change in the Line of Sight (*LoS*) angular measurement between the natural and controlled trajectory can lead to the observability of the system. Different metrics have been proposed in order to quantify the extent of such increment of the observability, based on geometric feature of the scenario. Specificaly, the approach where the observability is linked to the angular offset of the LoS unit vector in the non-controlled trajectory with the LoS of the controlled one, has been proven to be effective. In particular, such formulation can be easily implemented in the guidance optimal problem alongside any other guidance objective, such as the fuel expenditure. The work of the author presented in [3, 4] explored the applicability of such GNC strategy for the relative state observability enhancement in the extremely challenging environment of the rendez-vous with the LOP-G in the cislunar region. The approach has been proved to be successful in terms of error estimation performances and, consequently, of rendezvous execution capabilities. The goal of the current paper is to show the application of the same strategy in a different mission scenario, where instead of a rendez-vous mission, a bounded motion between two cooperative spacecraft (here still named *chaser* and *target*) is forsaken, remaining in the cislunar region, thus still targeting the environment of interest for the next decades lunar exploration missions. After this brief introduction, Section 2 will introduce the problem geometry and the GNC mathematical foundations. Section 3 will then present the results of the proposed application with two peculiar mission scenarios, providing also comments on the strategy's validity boundaries, before driving the final conclusions in Section 4.

2. Problem definition and GNC strategy

This section will introduce the basics of the Bearing-Only navigation strategy and the proposed architecture for the on-board Guidance Navigation and Control loop.

2.1 Bearing-Only geometry and rationale

In order to properly illustrate the bearing-only range detectability, Fig. 1 displays both the target, the grey dot fixed in the origin of the reference frame, and the chaser, red dot, before and after the execution of an observable manoeuvre. The figure represents also the observability angle θ, namely the angular distance between the two LoS unit-vectors with or without the control action. Ideally, with perfect measurements, the relative distance ρ can be obtained by trigonometry, but if a level of noise ε is introduced in the sensors, a perturbation in the range estimation $\delta\rho$ is added to the range estimation.

A useful design parameter for typical relative motion applications can be found in the relative range uncertainty itself. Following the work by Woffinden in [5], assuming small measurement errors, coming e.g. by the camera detector or by the image processing routines, this metric can be expressed as in Eq. (1).

$$\frac{\delta\rho}{\rho} = \frac{\varepsilon}{\sin\theta} \tag{1}$$

From such expression it is easily understood that two distinct ways to minimise the uncertainty are possible: either by improving the sensor accuracy or by maximising the observation angle θ. The former solution is unfortunately not always feasible due to technological limitations that provide a minimum value for ε below which it is quite difficult to go. Moreover, the philosophy behind bearing-only navigation techniques is definitely related to the exploitation of a single camera, which provides a great advantage from the economical perspective and from the simplicity of the hardware implementation. Consequently, from this simple formula it is possible to understand that

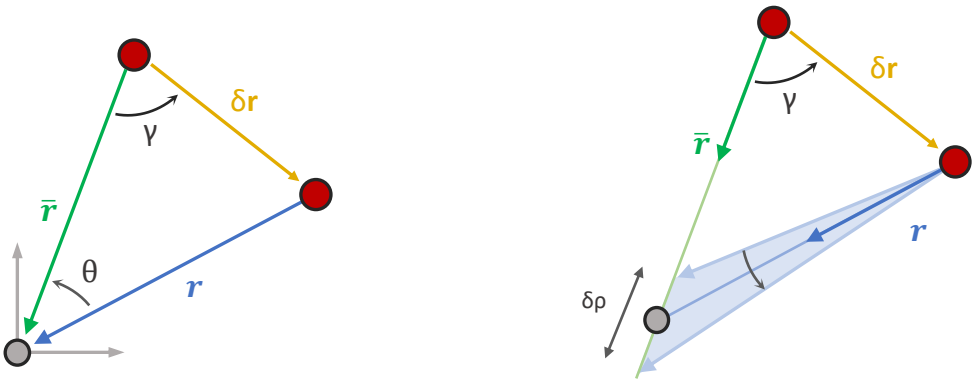

Figure 1: Range detectability geometry in the ideal (*left*) and real (*right*) scenario. $\mathbf{r}$ is the position vector of the real trajectory whereas $\bar{\mathbf{r}}$ represents the natural dynamics. Image readapted from [5].

the best approach for reducing the relative range estimation error is by looking at trajectory designs which maximise the value of θ. To perform that, however a specific Guidance and Control strategy has to be implemented which needs to be directly connected to the proposed navigation strategy. In the following subsection the details of the GNC architecture are introduced.

2.2 GNC Architecture

When dealing with a bearing-only architecture, the navigation process is directly influenced by the shape of the trajectory, therefore, it is mandatory to include inside the trajectory design a contribution that allows to improve the navigation performance. In this work, a Shrinking Horizon – Model Predictive Control (SH-MPC) is selected to compute the manoeuvres required to bring the spacecraft to a desired location. In this formulation, the trajectory is discretised into a series of points, arbitrarily spaced in time. However, differently from a standard MPC approach [6], with a shrinking horizon the transfer duration is fixed, and the problem is always solved from the current epoch until the final time, thus the time window shrinks at each re-optimisation according to the remaining optimisation time. The course of action for this kind of architecture is displayed in Fig. 2. Calling T_{rdv} the desired rendezvous time, the trajectory is discretised into n steps $t_M = [t_{M_1}, t_{M_2}, ..., t_{M_n}]$ and at each of those a manoeuvre is allowed. At the same time, the number m of reoptimisation performed along the trajectory is scheduled for $t_O = [t_{O_1}, t_{O_2}, ..., t_{O_m}]$ and is such that t_{O_i} does not necessarily equal t_{M_i}. Once the guidance is initialised, for each update time t_j it checks whether an optimisation is planned at the current epoch. If that is the case, the minimisation algorithms sets the estimated relative state as the initial point and searches a solution for the remaining discretisation points, eventually updating the manoeuvre scheme $\mathbf{U}_{opt}$. Afterwards, it also controls if a manoeuvre is planned; whenever that is the case, the chaser executes the control action according to $\mathbf{U}_{opt}$. Finally, the cycle is stopped when T_{rdv} is reached. Please notice that in a real implementation, it might not be feasible to solve the optimisation problem and execute a manoeuvre at the exact same epoch. Nevertheless, it is here assumed that the two tasks can be accomplished simultaneously.

2.3 Dynamic Model

The absolute dynamics of an object in the cislunar domain can be approximated as:

$$\mathbf{f}(\mathbf{x}) = \mathbf{a}_{3BP}(\mathbf{x}) + \mathbf{a}_{4th}(\mathbf{x}) + \mathbf{a}_{SRP}(\mathbf{x}) \qquad (2)$$

where $\mathbf{a}_{3BP}$ is the traditional Circular Restricted Three Body Problem (CR3BP) contribution and the remaining two terms are the perturbing effects of the Sun's gravitational force and the Solar Radiation Pressure (SRP), respectively. The relative translational dynamics is obtained from the derivative of the relative position vector of the chaser with respect to the target, denoted as $\mathbf{x}$:

$$\ddot{\mathbf{x}} = \ddot{\mathbf{r}}_c - \ddot{\mathbf{r}}_t \qquad (3)$$

where $\ddot{\mathbf{r}}_c$ and $\ddot{\mathbf{r}}_t$ are the absolute acceleration vectors of the two spacecraft. A useful approximation becomes available by linearising Eq. (3) with respect to the target state, holding true as long as the relative distance between the satellites is much smaller than

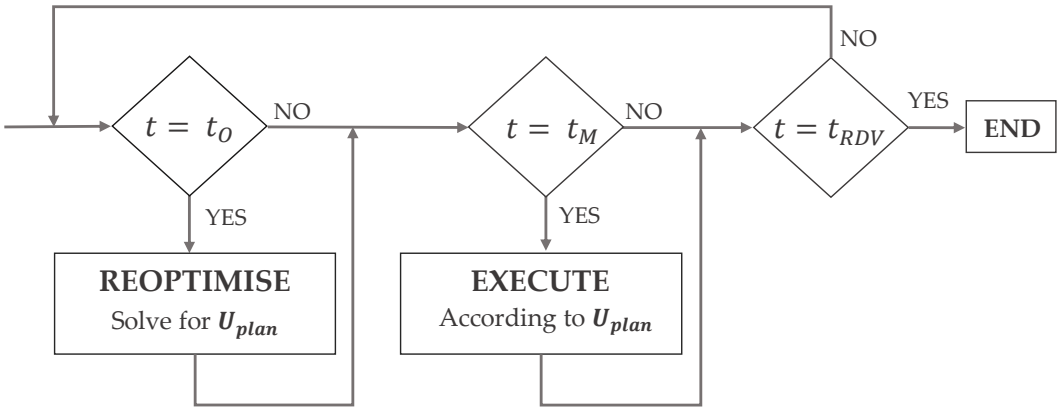

Figure 2: Guidance Flow-chart.

that between the target and the primaries [7]:

$$\begin{bmatrix} \dot{\mathbf{x}} \\ \ddot{\mathbf{x}} \end{bmatrix} = \mathbf{A}(\mathbf{x}_t(t)) \begin{bmatrix} \mathbf{x} \\ \dot{\mathbf{x}} \end{bmatrix} + \mathbf{B}(\mathbf{u} + \delta\mathbf{a}) \tag{4}$$

with $\mathbf{u}$ the control input and $\delta\mathbf{a}$ the perturbing accelerations. Since the matrix $\mathbf{A}$ depends on the absolute position of the target, the propagation of the relative dynamics requires knowledge of both the relative state and the absolute state of either spacecraft. To apply traditional linear control techniques and avoid an excessive computational burden, a closed-form analytical solution to system as in Eq. (4) is desirable, however such solution does not exist because the absolute dynamics of the target requires numerical integration. Nevertheless, a discrete-time solution over the time interval $[t_k, t_{k-1}]$ can be obtained by separating the free and forced contribution through the State Transition Matrix (STM) $\mathbf{\Phi}$ and the input matrix $\mathbf{G}$ [4]:

$$\mathbf{x}(t_k) = \mathbf{\Phi}(t_k, t_{k-1})\mathbf{x}(t_{k-1}) + \mathbf{G}(t_k, t_{k-1})\mathbf{u} \tag{5}$$

Notice that only in few cases the solution of the forced response (i.e., the convolution integral of the time-varying manoeuvre) can be expressed as the product between a matrix and a vector, as in Eq. (5). In this paper, such representation has been obtained assuming impulsive controls at the beginning of each time interval, making the input matrix readily available once the STM is known. Despite this hypothesis, the results presented in Section 3 will highlight that impulsive manoeuvres can also be used to approximate a low-thrust continuous control.

The model in Eq. (4) is a time-varying linear system, meaning that if $t_i \neq t_k$, then $\mathbf{\Phi}(t_k + \Delta t, t_k) \neq \mathbf{\Phi}(t_i + \Delta t, t_i)$ because the dependence of $\mathbf{\Phi}$ on the target state generates different results for different initial times as $\mathbf{x}_t(t_i) \neq \mathbf{x}_t(t_k)$. Therefore, even if a uniform time-step is adopted, $\mathbf{\Phi}$ must be computed at each discretisation point. To reduce the computational burden of such evaluation (the exact computation of $\mathbf{\Phi}$ and $\mathbf{G}$ requires the integration of 42 differential equations), the STM is approximated with a 2nd order Taylor series as:

$$\mathbf{\Phi}(t_k + \Delta t, t_k) = \mathbf{I}_6 + \mathbf{A}_k\Delta t + (\mathbf{A}_k^2 + \dot{\mathbf{A}}_k)\Delta t^2/2 \tag{6}$$

where $\mathbf{A}_k$ used to indicate the value of $\mathbf{A}(t)$ at time t_k.

2.4 Optimisation Problem

The optimisation problem to solve at each re-optimisation epoch is expressed as the minimisation of a fuel objective subject to both linear and non-linear constraints:

$$\begin{aligned} \min_{\mathbf{y}} \quad & \mathcal{J}_F(\mathbf{y}) && \text{(7a)} \\ \text{subject to} \quad & \mathbf{A}_{eq}\mathbf{y} = \mathbf{b}_{eq} \\ & \mathbf{A}_{iq}\mathbf{y} \leq \mathbf{b}_{iq} \\ & \mathbf{l}_b \leq \mathbf{y} \leq \mathbf{u}_b \\ & c(\mathbf{y}) \leq 0 \end{aligned}$$

where $\mathbf{y}$ is the vector of independent variables, containing the manoeuvres directions and, possibly, other associated quantities. $\mathbf{A}_{eq}$ and $\mathbf{A}_{iq}$ are the matrices that express the equality and inequality constraints, respectively. These become useful to bound the relative motion to specific regions of space and specify the boundary conditions; i.e., the initial and

final relative states. The lower $\mathbf{l}_b$ and upper boundaries $\mathbf{u}_b$ limit the solution search space and allow to account for system engineering limitations, such as the maximum thrust available. $c(\mathbf{y})$ is a non-linear constraint that forces a desired observability angle at a given epoch to aid the convergence of the navigation filter. Finally, $\mathcal{J}_F$ is the objective function used to represent the fuel consumption, either via a linear or quadratic expression of the optimisation variables. For what concerns the future notation, assuming the time-interval is discretised in n points, the relative states can be collected inside a vector $\mathbf{X} = [\mathbf{x}_1^T\ \mathbf{x}_2^T\ ...\ \mathbf{x}_n^T]^T$ of size $6n \times 1$. At the same time, a manoeuvre is admissible at every point but the last one, otherwise an additional relative state would be produced. Thus, in a similar fashion they are collected inside a global vector $\mathbf{U} = [\mathbf{u}_1^T\ \mathbf{u}_2^T\ ...\ \mathbf{u}_{n-1}^T]^T$ of size $3(n-1) \times 1$.

Fuel Objective

The fuel performance are traditionally quantified through the ΔV, unfortunately, such parameter can only be expressed as a non-linear function of the optimisation variables because it involves a square root by definition. In this work, two MPC workarounds are exploited, expressing J_F as a linear or quadratic function of the optimisation variables.

The most common approach is to is to exploit a quadratic objective J_{F_q}, written as function of $\mathbf{U}$ as [6]:

$$\mathcal{J}_{F_q} = \frac{1}{2}\mathbf{U}^T\mathcal{Q}\mathbf{U} \tag{8}$$

with $\mathcal{Q}$ a diagonal weighting matrix used to either prioritise or penalise the manoeuvres associated to certain epochs. The exploitation of a quadratic fuel objective usually guarantees a smooth control action and the resulting dynamics is more robust to disturbances and off-nominal conditions. However, the solution coming from the minimisation of this cost function may not be optimal in terms of overall fuel consumption [8]. Whenever this cost function is adopted, the optimisation vector $\mathbf{Y}$ is equal to the global manoeuvre vector $\mathbf{U}$.

A more realistic representation of the fuel expenditure is obtained by exploiting a 1-norm objective, i.e., the sum of the absolute values of all thrust elements inside $\mathbf{U}$:

$$\mathcal{J}_{F_s} = \sum_{k=1}^{3(n-1)} |\mathbf{U}_k| \tag{9}$$

This class of cost function generally yields solutions with smaller ΔV with respect to quadratic control objectives. Moreover, the manoeuvre plan consists of sparser control actions that are quite appealing if a continuous firing is not possible. The objective in Eq. (9) is a piece-wise linear function and a conversion is desirable to efficiently solve the optimisation problem. Therefore, the optimisation vector $\mathbf{Y}$ is augmented with a new set of variables $\mathbf{S} = [\mathbf{s}_1^T\ \mathbf{s}_2^T\ ...\ \mathbf{s}_{n-1}^T]^T$, named *slack variables* [9]. Then, by adding specific inequality constraints, each of the elements inside $\mathbf{S}$ can be set equal to the absolute value of the corresponding element in $\mathbf{U}$. Defining $\mathbf{Y} = [\mathbf{U}^T\ \mathbf{S}^T]^T$ the augmented optimisation vector, the cost function in Eq. (9) is written as:

$$\mathcal{J}_{F_s} = \mathbf{F}^T\mathbf{Y} \tag{10}$$

where the vector $\mathbf{F}$ has the first $3(n-1)$ elements equal to zero and the remaining set to one. To ensure $\mathbf{S}$ equals the absolute value of $\mathbf{U}$, all the individual constraints are grouped through a matrix as:

$$\mathbf{A}_s\mathbf{Y} \leq \mathbf{0}_{2m} \quad \text{where} \quad \mathbf{A}_s = \begin{bmatrix} \mathbf{I}_m & -\mathbf{I}_m \\ -\mathbf{I}_m & -\mathbf{I}_m \end{bmatrix} \tag{11}$$

with $m = 3(n-1)$. This representation becomes particularly useful when fuel-optimal trajectories are sought because it allows to solve the optimisation problem with a linear programming algorithm.

Boundary Conditions

A desired destination point is enforced by writing the final position as function of the global manoeuvre vector $\mathbf{U}$ and of the initial conditions:

$$\mathbf{x}_n = \mathbb{G}\mathbf{U} + \mathbb{A}_{1n}\mathbf{x}_1 \tag{12}$$

where $\mathbf{x}_1$ is the initial point and $\mathbb{A}$ is defined as:

$$\begin{aligned} \mathbb{A}_{ij} &= \prod_{k=i}^{j-1} \mathbf{\Phi}_k \ \text{ if } j > i \\ \mathbb{A}_{ij} &= \mathbf{I}_6 \ \text{ if } j \leq i \end{aligned} \tag{13}$$

and $\mathbb{G}$ is a $6 \times m$ matrix equal to:

$$\begin{aligned} \mathbb{G} &= \begin{bmatrix} \mathbb{G}_1 & \dots & \mathbb{G}_{n-1} \end{bmatrix} \\ \text{with} \quad \mathbb{G}_j &= \mathbb{A}_{(j+1)n}\mathbf{G}_j \end{aligned} \tag{14}$$

The equality constraint is then expressed as follows:

$$\begin{aligned} \mathbf{A}_{BC}\mathbf{Y} &= \mathbf{b}_{BC} \\ \mathbf{b}_{BC} &= \hat{\mathbf{x}}_{EC} - \mathbb{A}_{1n}\mathbf{x}_1 \end{aligned} \tag{15}$$

where $\hat{\mathbf{x}}_{EC}$ is the desired final point. Whenever the quadratic objective $\mathcal{J}_q$ is used, $\mathbf{A}_{BC}$ equals the matrix $\mathbb{G}$ defined in Eq. (14), otherwise it must be properly expanded to account for the presence of the slack

variables inside the optimisation vector [3,4]. Finally, thrust magnitude constraints are straightforwardly added through the lower and upper bound vectors.

Non-linear Observability Constraint

In Section 2.2 it was highlighted that to minimise the relative range navigation error, the observability angle θ should be maximised. The easiest and most efficient way to implement such parameter inside the optimisation problem is to introduce a non-linear constraint, demanding that after M steps the observability angle should be greater or equal than a given threshold. The number of steps can be used as an additional tuning parameter. Mathematically, the constraint is expressed as:

$$c(\mathbf{U}) = \theta_{\text{THR}} - \cos^{-1}\left(\frac{\bar{\mathbf{x}}_M^T \mathbf{x}_M(\mathbf{U})}{\|\bar{\mathbf{x}}_M\|\|\mathbf{x}_M(\mathbf{U})\|}\right) \leq 0 \quad (16)$$

where $\bar{\mathbf{x}}_M$ depends only on the initial conditions. By formulating this constraint as an inequality, the solver will automatically find the solution with the lowest fuel consumption among all the possible values of $\theta \geq \theta_{\text{THR}}$. The two vectors in the previous expression are easily computed as:

$$\begin{aligned} \bar{\mathbf{x}}_M &= \mathbb{A}_{1M}\mathbf{x}_1 \\ \mathbf{x}_M &= \bar{\mathbf{x}}_M + \mathbb{G}_M\mathbf{U} \end{aligned} \quad (17)$$

The matrix $\mathbb{G}_M$ is similar to Eq. (14) but is evaluated only up to the $(M-1)$-th term:

$$\begin{aligned} &\mathbb{G}_M = \begin{bmatrix}\mathbb{G}_1 & \dots & \mathbb{G}_{M-1} & \mathbf{0} & \dots & \mathbf{0}\end{bmatrix} \\ &\text{with} \quad \mathbb{G}_j = \mathbb{A}_{(j+1)M}\mathbf{G}_j \end{aligned} \quad (18)$$

The evaluation of the non-linear constraint can be accelerated by pre-computing these matrices.

3. Simulation and Results

To assess the capability of the proposed architecture to improve the relative state estimation of a satellite, the SH - MPC guidance is tested in a closed-loop system along with a navigation filter, as shown in Fig. 3. The selected scenarios involve two spacecraft flying on heterogeneous non-keplerian orbits, with distances in the order of thousands of kilometres. Since it is here desired that the chaser remains bounded to its nominal orbit, the final boundary conditions of the optimisation problem are set to guarantee that at the end of the relative navigation phase the chasing spacecraft finds himself on its original orbit, as if nothing had happened. A high-fidelity propagator is used to model the chaser and target absolute dynamics, together with the perturbing effects of the Sun gravitational force and the Solar Radiation Pressure (SRP). As the propagation of the relative dynamics in the navigation filter requires knowledge of the target dynamics, it is here supposed that at each re-optimisation epoch, an uncertain estimate of the target absolute state is transmitted to the chaser. Then, exploiting the results of [3], a time-invariant approximation of the STM is adopted to predict the relative dynamics evolution until the next re-optimisation occurs. An Unscented Kalman Filter (UKF) is used to re-construct the relative state, with an update frequency of 0.1 Hz. Finally, to stress the architecture robustness and statistically evaluate the navigation performance, 100 Monte Carlo simulations are run for each scenario, changing the filter initialisation and the noise effects.

3.1 DRO to Lyapunov Navigation

The chaser is settled on a L2 Lyapunov while the target is on a Distant Retrograde Orbit (DRO), with an initial distance between the spacecraft of 5300 km. The navigation filter is initialised with relative position and velocity uncertainties of 10% and 2.5%, respectively. The effects of three different desired observability angles are analysed in the following figures. Simultaneously, a comparison between the two fuel cost functions is performed representing high and low-trust engines with the linear and quadratic objectives, respectively. Notice that as the final state is selected on the original nominal orbit, the observability angles at the end of the simulation are always null. Therefore, the constraint on the observability angle has been imposed in the middle of the simulation because the resulting symmetry guarantees the lowest fuel consumption. The two engines result in similar navigation performance, although the low-thrust always requires an extra 10 m/s. The lowest relative error (the yellow line) is around the 0.4% of the range, which corresponds to approximately 60 km; 10 times lower than the original value. Interestingly, for the impulsive case the greater improvements in the relative navigation error happen immediately after the execution of the manoeuvres, and then remain approximately constant throughout the whole coasting phase. However, since the distance between the spacecraft keeps increasing, the absolute estimation error increases as well. Indeed, throughout the simulation the range constantly increases from the initial 5300 km up to 16.500 km.

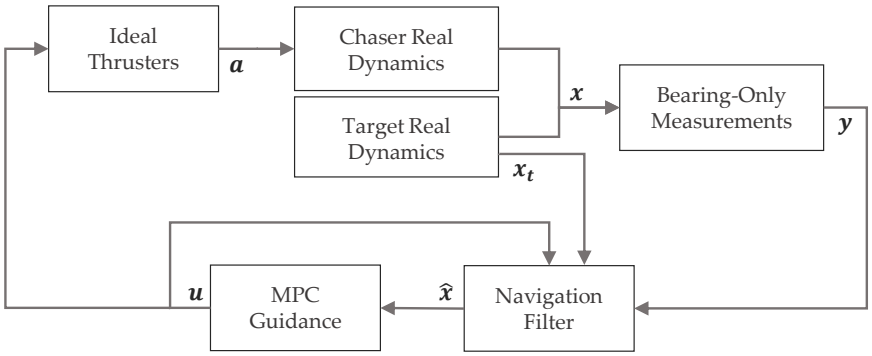

Figure 3: Simulation environment.

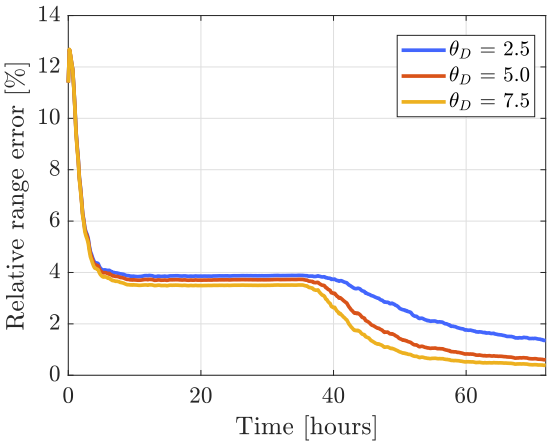

Figure 4: Impulsive - Relative position error.

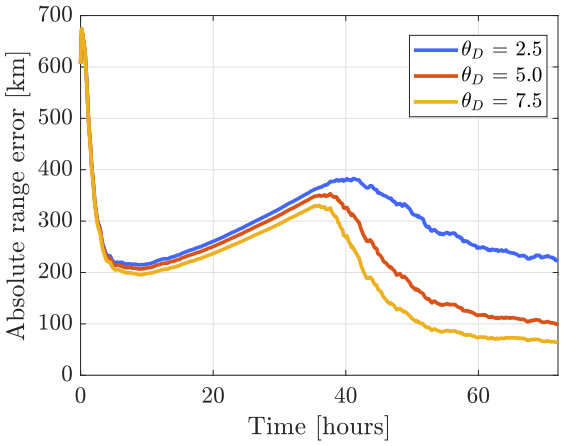

Figure 6: Impulsive - Absolute position error.

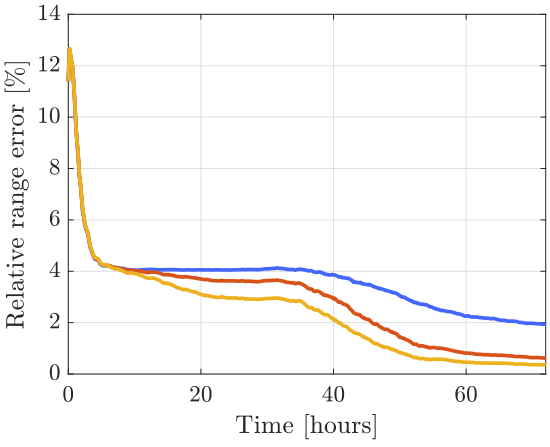

Figure 5: Low-thrust - Relative position error.

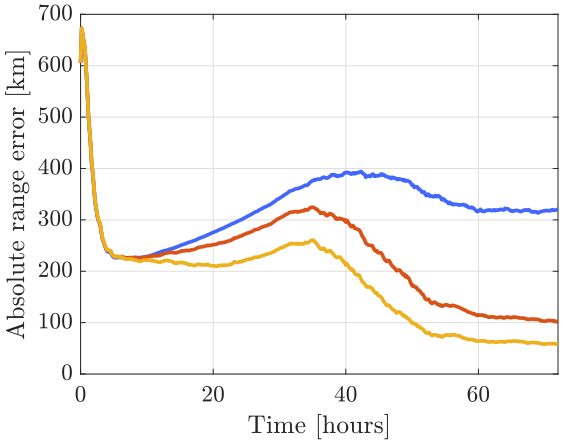

Figure 7: Low-thrust - Absolute position error.

Figure 9 shows that by solving for the quadratic fuel objective, the impulsive approximation of the forced response effectively approximates the behaviour of a low-thrust continuous control. This result is extremely useful since the convolution integral of a generic continuous thrust vector $\mathbf{u}(t)$, cannot be written in discrete form as the product between a matrix and a vector. Thus, the quadratic objective makes possible to model a pseudo low-thrust control within a discrete-time framework.

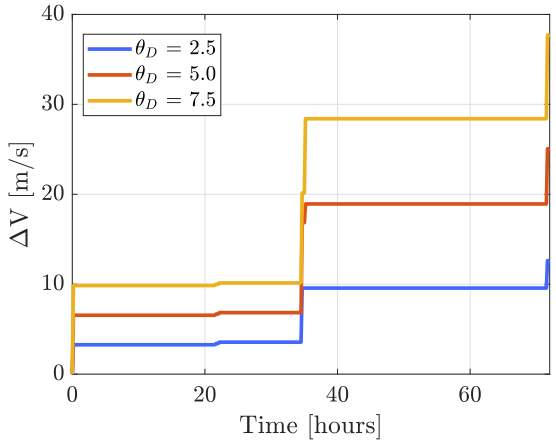

Figure 8: Impulsive - ΔV.

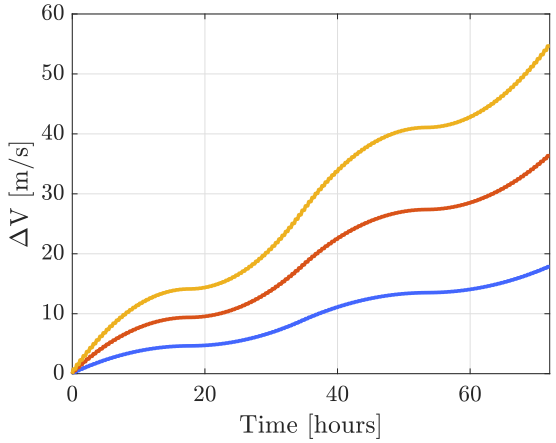

Figure 9: Low-thrust - ΔV.

A few considerations can be extrapolated from these outcomes. When the goal is to reduce the absolute uncertainty below a given threshold, various possibilities are available. If the target is fixed (i.e., the relative distance), the necessary observability angle is directly obtained from Eq. (1). On the other hand, if different spacecraft can be exploited as a target for measurements, it is more convenient to choose the one that is closer to the chaser.

3.2 Halo to DRO Navigation

In the previous scenario, a high relative distance was selected with the sole purpose of proving the validity of the Guidance and Navigation (GN) architecture. However, it is always desirable to work with smaller values because, given the angle θ, the ΔV required to perturb the natural trajectory grows as function of the range between the spacecraft. In the following simulation the chaser has been placed on a L2 Halo orbit, whereas the location of the target has remained unchanged. Thus, the resulting relative motion will include both in-plane and out-of-plane components. Additionally, the initial positions have been selected to generate a relative motion whose range gradually reduces in time (contrary to the previous configuration). The optimal manoeuvre plan was computed assuming a high-thrust engine and a desired minimum observability angle of 1 degree.

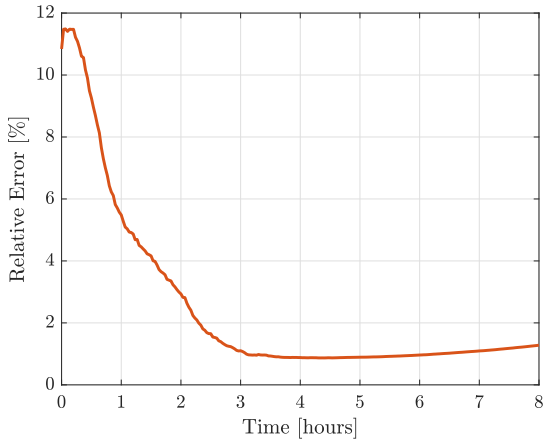

Figure 10: Relative position error.

Figure 10 shows that despite a small observability angle was selected, the navigation filter is capable of improving the initial error up to 1% of the range. As visible in Fig. 12 the distance steadily decreases throughout the first half of the simulation; thus from an absolute point of view, the position error drops from more than 700 km to just 20 km. Then, as the satellites move away from each other, the absolute error deteriorates accordingly. Interestingly, in this scenario the filter convergence is almost exclu-

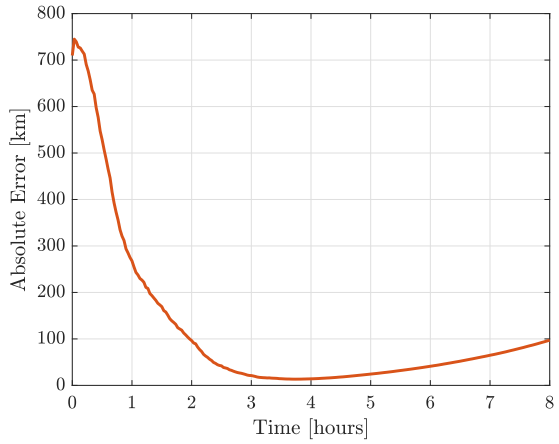

Figure 11: Absolute position error.

sively due to the range reduction: enforcing higher observability angles yields only minor navigation improvements, which are not worth the extra-fuel consumption. Therefore, a careful selection of the natural relative motion can provide potential trajectories that enhance the filter observability with minimum fuel consumption. Indeed, thanks to both the smaller distance and lower observability angle, the total ΔV required is only of 4.58 m/s, less than half the smallest value of the previous case. Notice that

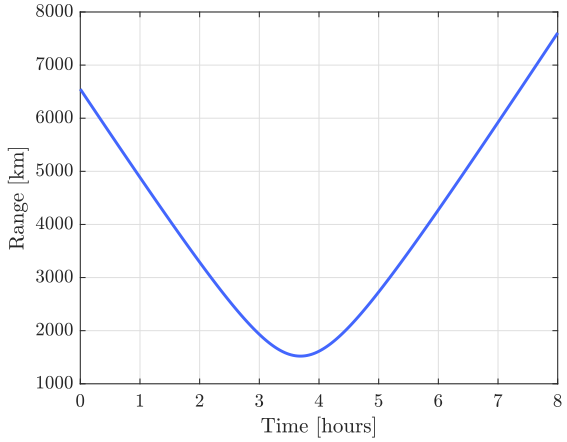

Figure 12: Range evolution.

towards the end of the simulation, Fig. 10 displays an increment of the relative error, contrary to Fig. 4 and 5 which are characterised only by constant or decreasing sections. This issue is associated with the quality of the linear approximation adopted to predict the relative dynamics. Indeed, the linearisation of the original non-linear relative system was carried out assuming the range between the satellites to be much smaller than the target-Moon distance. The ratio between these two values, named *error index*, can be used as a reference for the quality of the linear approximation and has been reported in Fig. 13. By comparing these results with the relative position error, the final performance reduction can be correlated with the linear approximation deterioration. As the error index gets worse, the model accuracy declines and the relative error grow rate increases (i.e., the faster increment at the end is caused by a worse relative model quality). As a reference, the previous simulation scenario had an accuracy index of 2.5%. Unfortunately, this parameter drastically reduces the

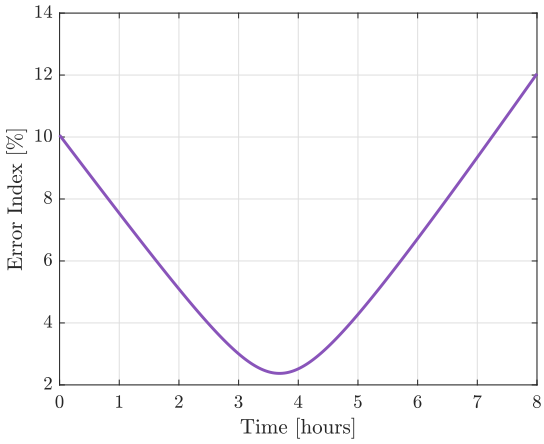

Figure 13: Linear model error index.

potential orbital combinations that can be exploited with the proposed architecture. For example, when selecting orbits belonging to different non-keplerian families, there are only few points where the error index is small enough to guarantee the convergence of the navigation filter. The results prove that an error index smaller than 10% is enough to provide an improvement of the initial error, whereas a value below 5% is recommended to guarantee that the relative error remains within a bounded interval.

4. Conclusions

The present work has analysed the applicability of bearing-only navigation to improve the relative state estimation of a spacecraft in the cis-lunar environment. The effectiveness of the proposed quasi-autonomous SH-MPC architecture were explored in

two case studies: a planar DRO to L2 Lyapunov navigation and a DRO to Halo relative motion. In both cases, the GNC scheme has proven capable of computing observable relative trajectories through the concept of observability angle, reducing the relative error to a small fraction of the initial value. A strategy to approximate low-thrust trajectories was presented, showing that despite the convolution integral of the forced response is simplified under the assumption of impulsive manoeuvres, the adoption of a quadratic fuel objective generates trajectory with a piece-wise continuous and smooth control action. Finally, the characteristics of potential low-ΔV trajectories were identified, together with the boundaries in which the linear approximation holds. The outcomes of this paper broaden the range of operations for which angle-only measurements can successfully be exploited, from close-range rendezvous to long-range scenario, opening the door to a variety of missions that entail solving for the relative dynamics in multi-gravitational environments.

References

[1] D. C. Woffinden and D. K. Geller. Observability criteria for angles-only navigation. *IEEE Transactions on Aerospace and Electronic Systems*, 45(3):1194–1208, 2009.

[2] J. Grzymisch and W. Fichter. Observability criteria and unobservable maneuvers for in-orbit bearings-only navigation. *Journal of Guidance, Control, and Dynamics*, 37(4):1250–1259, 2014.

[3] M. Ceresoli, G. Zanotti, and M. Lavagna. Bearing-only navigation to support proximity operations on cislunar non-keplerian orbits. In *SpaceOps 2021 Virtual Edition*, Cape Town, South Africa, 2021.

[4] M. Ceresoli. Bearing-Only Strategies for Proximity Navigation on Cislunar Orbits. Master's thesis, Politecnico di Milano, Dipartimento di Scienze e Tecnologie Aerospaziali, Milano, Italy, 2021.

[5] D. C. Woffinden and D. K. Geller. Optimal orbital rendezvous maneuvering for angles-only navigation. *Journal of guidance, control, and dynamics*, 32(4):1382–1387, 2009.

[6] S. Silvestrini, J. Prinetto, G. Zanotti, and M. Lavagna. Design of robust passively safe relative trajectories for uncooperative debris imaging in preparation to removal. In *2020 AAS/AIAA Astrodynamics Specialist Conference*, pages 1–18, Virtual Lake Tahoe, United States, 2020.

[7] L. Bucci, A Colagrossi, and M. Lavagna. Rendezvous in lunar near rectilinear halo orbits. *Advances in Astronautics Science and Technology*, 1(1):39–43, 2018.

[8] Hartley, Edward N. A tutorial on model predictive control for spacecraft rendezvous. In *2015 European Control Conference (ECC)*. IEEE, 2015.

[9] J. Grzymisch and W. Fichter. Optimal rendezvous guidance with enhanced bearings-only observability. *Journal of Guidance, Control, and Dynamics*, 38(6):1131–1140, 2015.